INSTITUTE FOR NUCLEAR STUDY
UNIVERSITY OF TOKYO
Tanashi, Tokyo 188
Japan

INS-Rep. -1000
July 1993

INS--1000

JP9402184

Exotic Aspects of Hadronic Atoms - Anomalous Quasi-Stabilities

Toshimitsu Yamazaki

Institute for Nuclear Study
University of Tokyo
3-2-1, Midori-cho, Tanashi, Tokyo 188, Japan

Exotic Aspects of Hadronic Atoms - Anomalous Quasi-Stabilities

Toshimitsu Yamazaki

Institute for Nuclear Study
University of Tokyo
3-2-1, Midori-cho, Tanashi, Tokyo 188, Japan

Abstract

Recently revealed, but hitherto unknown, new aspects of hadronic atoms, namely, anomalous quasi-stabilities of negative hadrons, are discussed. One is on long-lived antiprotonic helium atoms, characterized as "atomic exotic halo" and the other is on deeply bound pionic atoms, characterized as "nuclear exotic halo".

1 Introduction

The hadronic atom is a special atom composed of a negatively-charged hadronic particle X^- and a nucleus of charge $+Ze$. They are combined by the Coulomb attraction, forming Bohr orbitals with principal quantum number n and orbital angular momentum l. The binding energy is expressed by a well known Bohr formula

$$E(n,l) = -Z^2 \frac{M}{m_e} \frac{1}{n^2} Ry \tag{1}$$

where

$$Ry = \frac{m_e e^4}{2\hbar^2} = 13.6 \text{ eV}. \tag{2}$$

The energy levels are scaled by the reduced mass M of X^-, and proportional to Z^2. They are degenerate for a given n and different $l = 0, 1, 2, ..., n-1$. This $n-$fold degeneracy is characteristic of a two-body Coulomb atom with a point nucleus, and is removed when any change of this situation takes place, such as the effect of atomic electrons and of finite nuclear size.

The size of the Bohr orbital is given by

$$\langle r_X(n) \rangle = n^2 \frac{m_e}{M} \frac{1}{Z} a_B, \tag{3}$$

where

$$a_B = \frac{\hbar^2}{m_e e^2} = 0.53 \times 10^{-8} \text{cm}. \tag{4}$$

It is scaled by m_e/M and by $1/Z$. This means that a typical hadronic Bohr orbital lies somewhere between the electronic orbital and the nuclear surface.

The exotic atom is formed by a capture reaction as

$$X^- + [Z]^0 \rightarrow (X^-[Z]^+)_{nl} + e^-, \tag{5}$$

namely, an incoming X^- ionizes one of the atomic electrons of a neutral target atom $[Z]^0$ to an ionized state $[Z]^+$ by which X^- is bound to form a state (n, l). The most likely state initially formed is often said to be given by the condition that the orbital size of X^- is equal to that of the ionized electron $\langle r_X(n)\rangle \sim \langle r_e\rangle$. If a K-shell electron is ionized, the equality

$$n^2 \frac{m}{M} = 1 \tag{6}$$

yields the famous estimate for the most probable n:

$$n = n_0 \equiv (M/m)^{1/2}. \tag{7}$$

This condition is equivalent to another condition that the binding energy of the formed X^- orbital be equal to that of the ionized electron.

The above estimate has, however, not been tested so far, because those initial states are usually *invisible*. They proceed to lower bound states via further Auger processes and eventually via radiative transitions, whichever faster. What we can observe is a series of x-ray cascade after X^- reaches a lower bound state.

The precision spectroscopy of muonic x-rays has provided detailed knowledge of the nuclear charge radius and its distribution because μ^- can cascade down to the ground state, which is located in the nuclear surface region. In the case of hadronic atoms, however, the situation is quite different; as soon as X^- feels the strong interaction from the nucleus, it is quickly absorbed by the nucleus and the x-ray cascade terminates there. The "last orbital", where the x-ray cascade terminates, is characterized by the condition that the absorption width Γ_{abs} be equal to the x-ray cascade width Γ_{rad}. Since the strong interaction has an imaginary part, whose strength is about 10 MeV, a hadronic orbital which is located as far as 10 times the nuclear surface has an absorption width as much as 10 keV, which eats up the radiative width. So, $\langle r_X\rangle = 10R_N$ is a rough criteria for the last orbital. X-ray spectroscopy for last orbitals provides experimental information on the strong-interaction shift ΔE_{nl} and width Γ_{nl}. These are the most important sources of information on the strong interaction potential.

It is obvious that no x-ray spectroscopy is possible for inner bound states. For instance, pionic x-ray spectroscopy has found that the $4f$ (or possibly $3d$) state is the last orbital in ^{208}Pb. Then, how and where do the $2p$ and $1s$ states exist? This very natural question had not been raised presumably due to the prevailing misbelief that no such inner states do exist. Toki and Yamazaki [1,2] pointed out in 1988 that such inner states are expected to exist with narrow widths for pions and can be produced by suitable nuclear reactions.

The present situation of hadronic atoms is illustrated in Fig. 1. So far, the intermediate region has well been studied experimentally, but neither the initial region $\langle r_X\rangle \sim \langle r_e\rangle$ nor the inner region $\langle r_X\rangle < 10R_N$ has been touched upon. Recently, the Tokyo group discovered new phenomena that the initially formed hadronic states in helium media are metastable [3–5]. These discoveries have provided the first opportunity to study the initial region. In this lecture the author describes these new developments.

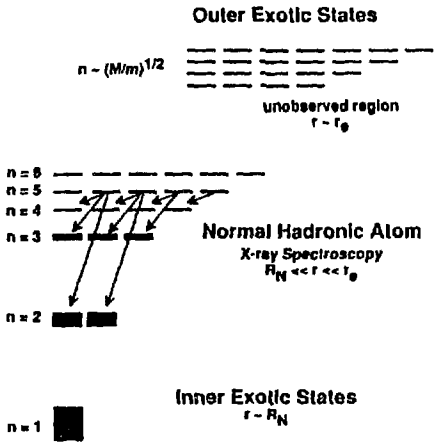

Fig. 1. Overview of hadronic atoms. The entry region in the case of helium constitutes metastable "exotic atomic halo", while the deeply bound region in heavy nuclei may probably constitute Coulomb-assisted "exotic nuclear halo" of anomalously narrow widths, if the negative hadron feels repulsion from the nucleus.

2 Discovery of Metastability of Hadronic Helium Atoms

While the SKY group of the University of Tokyo at KEK was searching for Σ hypernuclei to be produced by (stopped K^-, π) reactions in liquid helium [6], they encountered a suprising fact that striking peaks appeared at 205 MeV/c and 235 MeV/c in a momentum spectrum of negatively-charged particles [3]. They were immediately identified as characteristic two-body decay products of K^-; $K^- \rightarrow \pi^- + \pi^0$ and $K^- \rightarrow \mu^- + \bar{\nu}_\mu$, respectively. Any negative hadron is subject to common fate to immediate death after strong nuclear capture, which usually takes place in a picosecond after hadronic-atom formation. Therefore, there is only a very little time for any negative hadron stopped in matter to undergo free decay of lifetime τ_{free}. Contrary to this belief, they found the existence of free-decay products of about 2 % branching [3].

Later they learned that old experiments in helium bubble chambers had found anomalous free decays of π^- and K^- of 2 % fraction. See Hayano *et al.* [7] for historical accounts of this problem. At that time these fractions f were used to deduce "average cascade times" in such a way that $T_{av} = \tau_{free} \times f$. The T_{av} thus deduced from this "homogeneous-process" interpretation turned out to be 10^{-10} sec, which is by two orders of magitude slower than the theoretical expectation. On the other hand, Condo [8] proposed a totally different interpretation (can be called "inhomogeneous-process" model) that negative hadrons of this fraction are trapped by long-lived atomic orbitals.

Condo pointed out this possibility with reasoning that large-l states of the initially formed neutral hadronic atoms, $e^- X^- He^{++}$ (to be often described as $X^- He^+$), cannot decay by fast Auger transitions, because the $\Delta l = 1$ transition energies are smaller than

the electron ionization energy, $I_0 = 25$ eV, of helium atom. Furthermore, the neutrality of this atom including one electron makes the Stark mixing with other helium atoms less likely. Russell [9] made theoretical calculations for the structure and transition probabilities based on the variational method. He found that the near circular orbitals of $X^- He^+$ have long lifetimes (in the case of $\bar{p}$ the lifetime is as long as 1 μsec), but of course this calculation should apply to ideally isolated atoms, not to those in condensed matter like liquid helium. Since $\bar{p}p$ atoms are known to quench in hydrogen gas [10] as well as the metastable $2s$ μ^-He atoms [11] in helium gas, one hardly believed such metastability to persist in liquid helium.

So, this interesting possibility had remained untouched experimentally until the accidental encounter in 1989 by the SKY experiment [3]. They found the two monoenergetic components in a delayed spectrum (Fig. 2), revealing that the lifetime is around 10 nsec compared with the free lifetime of $K^{\pm}$ of 12 nsec. The overall lifetime of the trapping states was thus deduced to be 50 nsec or so. Outa *et al.* [12] found a shorter lived component from K^- absorption products.

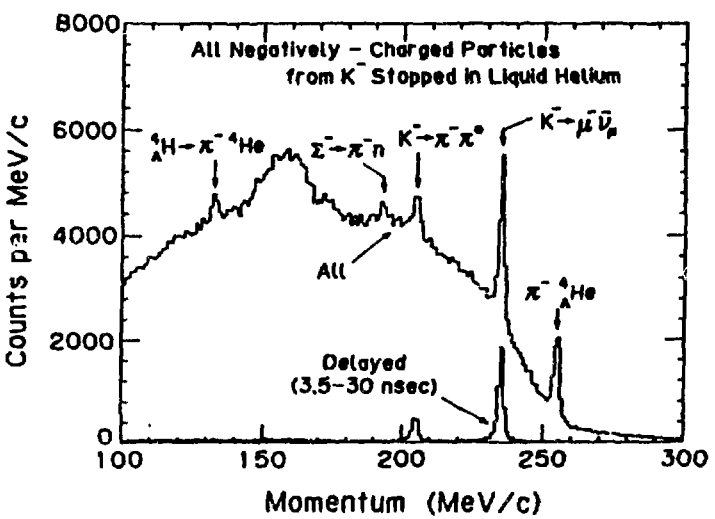

Fig. 2. Prompt and delayed momentum spectra of all negatively charged particles emitted from K^- stopped in liquid helium. The delayed spectrum revealed the existence of metastable states of overall trapping lifetime of 50 nsec [3].

Nakamura *et al.* [4] searched for a similar phenomena for π^- at TRIUMF. They found that delayed protons are emitted after π^- absorption in liquid helium. The overall trapping lifetime was determined to be 10 nsec.

What would happen for antiprotons? Spectacular phenomena might be revealed, because the mass of $\bar{p}$ is large and furthermore, $\bar{p}$ is stable in free space, and thus, has an unlimited time window. Iwasaki *et al.* [5] searched for delayed annihilation products (charged pions) after $\bar{p}$ stopping in liquid helium using an antiproton beam from KEK. They discovered that about 3 % of stopped antiprorons are subject to delayed annihilation, showing a multi-component exponential decay with an average lifetime of about 3 μsec. Antiprotons do survive as long as 10 μsec.

The observed metastability is certainly connected with the structure of X^-He^+. Yamazaki and Ohtuki [13] made further theoretical accounts of the phenomena. The metastable $\bar{p}He^+$ atom and its level structure are illustrated in Fig. 3. The initial quantum number n_0 is around 38 in the case of $\bar{p}$ in ^{4}He. The electron in its 1s state is quantum-mechanically distributed, while the $\bar{p}$ of $(n, l) = (38, 37)$ is localized and is circulating around the nucleus with a frequency much smaller than the electron frequency. The electron cloud tends to follow the motion of $\bar{p}$, and is slightly polarized in the direction opposite to $\bar{p}$. This $\bar{p}He^+$ atom looks like i) an exotic helium atom with replacement of one e^- by $\bar{p}$ at high quantum states keeping the same energy, ii) an exotic hydrogen with a "giant pseudo proton" of $\bar{p}He^{++}$, and iii) an exotic diatomic molecule with two "nuclei", one is He^{++}, the other, $\bar{p}$, has a charge of -1. We called this exotic atom "atomcule". Its presence in condensed matter and its reaction with other atoms/molecules are very intriguing subjects to study. The KEK experiment raised a number of questions.

1. Why are the metastable states stable against collisions in liquid helium? What is the effect of dense medium on the lifetimes and trapping fractions?
2. Why are the metastable states populated? What gives the trapping fraction f?
3. What is the precise shape of the time spectrum? How is it explained theoretically?
4. Is there any isotope effect between ^{4}He and ^{3}He?
5. Any such metastability in other atoms?

In order to obtain further information on this exotic metastability we have to study the phenomena in various phases of helium. For this purpose a series of new experiments have been undertaken and carried out by using the Low Energy Antiproton Ring (LEAR) at CERN.

3 CERN Experiment PS205

A new experimental group PS205 was formed, which started a series of experiment at CERN in 1991. LEAR provides an ideal antiproton beam for this purpose. It is monoenergetic and low energy. This means that we can stop antiprotons in a localized space even in a gas target. With a beam of 100 MeV/c momentum the total range is about 50 g/cm^2 and its distribution is about 0.5 mg/cm^2. It is only a few cm in 3-bar helium gas! The beam spot was as small as a few mm. This fantastic beam permitted us to carry out the measurement of time spectra of annihilation pions in various gas medium.

One beam spill contains $10^8 \sim 10^9$ $\bar{p}$'s, which are slowly extracted over 1000 sec, yielding $10^5 \sim 10^6$ $\bar{p}$'s/sec. We used a small fraction of the beam as a parasitic user. Since our time window spans 50 μsec, we did not need more than 10^4 $\bar{p}$/sec. The experimental set up used in 1992 is shown in Fig. 4. The incoming $\bar{p}$ is detected by a very

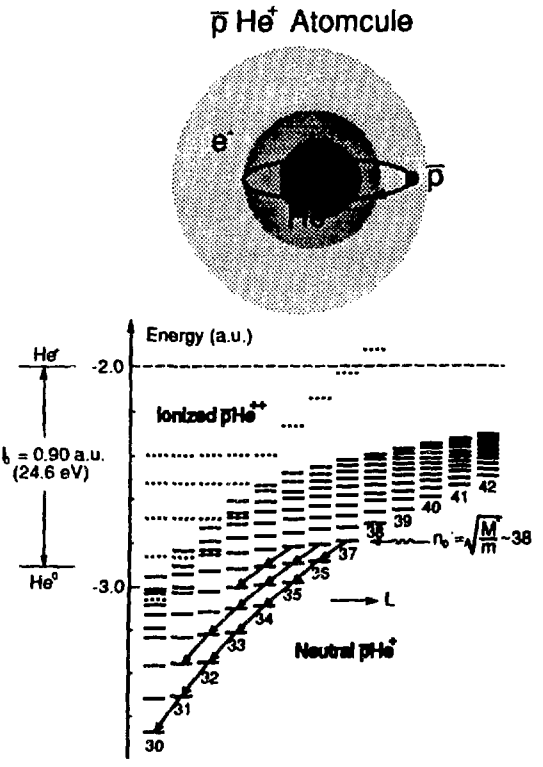

Fig. 3. Energy diagram of metastable antiprotonic helium atomcule. The levels expressed by bold lines are metastable, while those by broken lines are fast decaying states. Calculated by K. Ohtsuki. Taken from [14].

thin (100 μm thick) plastic scintillator, which is located just before a target gas chamber. Pions emitted from the target were detected by arrays of scintillator telescopes. The time between the arrival of $\bar{p}$ and the emission of pions was measured by using multi-stop Time to Digital Converters (Lecroy TDC4208).

This seemed to be straightforward in principle, but in practice we had to solve the following problems. The most serious is how to remove fake delayed events. Prompt annihilation events which occur within the time gate of 50 μsec produce fake "delayed pions" ($n_{\rm fake}/N_{\rm beam} = N_{\rm beam} \cdot T_{\rm gate}$ = order of 1, while the true delayed fraction is of order of 0.03!). To cut this type of fake events we used the information of "second $\bar{p}$", namely, when a second $\bar{p}$ arrives within the time gate, such an event was rejected. However, since the efficiency of the counter B is not 100 %, some escaped from this rejection.

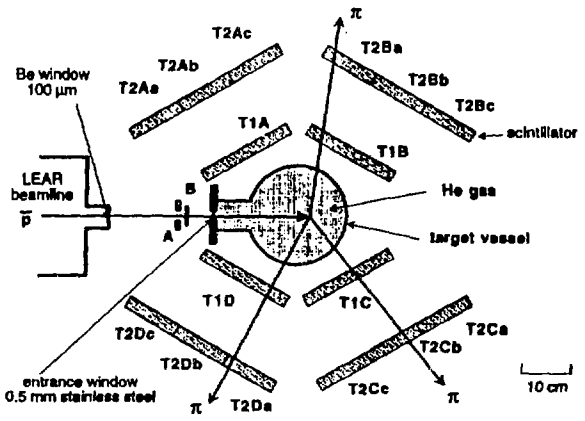

Fig. 4. Setup of the PS205 experiment at CERN-LEAR in 1992.

Another type of fake events arose from secondary e^+ emitted from prompt π^+ stopped somewhere in the vicinity of the target and the counters via the $\mu^+ \rightarrow e^+$ process with a mean life time of 2.2 μsec. To remove this we required coincidence of 2 or 3 simultaneous delayed particles.

The first CERN experiment thus carried out was very successful. We obtained time spectra of delayed annihilation of $\bar{p}$ stopped in gaseous helium. A brief report of the results was published [14]. It took only one hour to obtain a good enough time spectrum (at KEK it took one week of beam time even for liquid helium!) and the fake deleyed events were completely suppressed. Some typical time spectra are shown in Fig. 5 and 6.

The most surprising observation is that the time spectrum for pure ^{4}He gas looks very much like that taken at KEK for liquid helium. The average lifetime was 3 μsec, but the good statistics allowed us to recognize that the time spectrum is not a sum of expenential functions, but shows a growth-decay type bending that is characteristic of chain decay through 2 or more metastable states. Phenomenologically, we define the average lifetime for a given time interval $t_0 < t < t_{max}$ as follows.

$$T_{av}(t_0, t_{max}) = \frac{\int_{t_0}^{t_{max}} t \cdot N(t)dt}{\int_{t_0}^{t_{max}} N(t)dt} - t_0 \qquad (8)$$

The lifetime does not depend much on the pressure.

We observed a significant isotope effect between ^{4}He gas and ^{3}He gas, as shown in Fig. 5. The lifetime for ^{3}He is 13 % shorter than for ^{4}He. This observation is in good agreement with that expected from the difference in the reduced mass of $\bar{p}$ (see section 7).

Another interesting finding is that the delayed component is quenched by adding a very small amount of hydrogen and other impurity gasses. The effect is shown in Fig. 6.

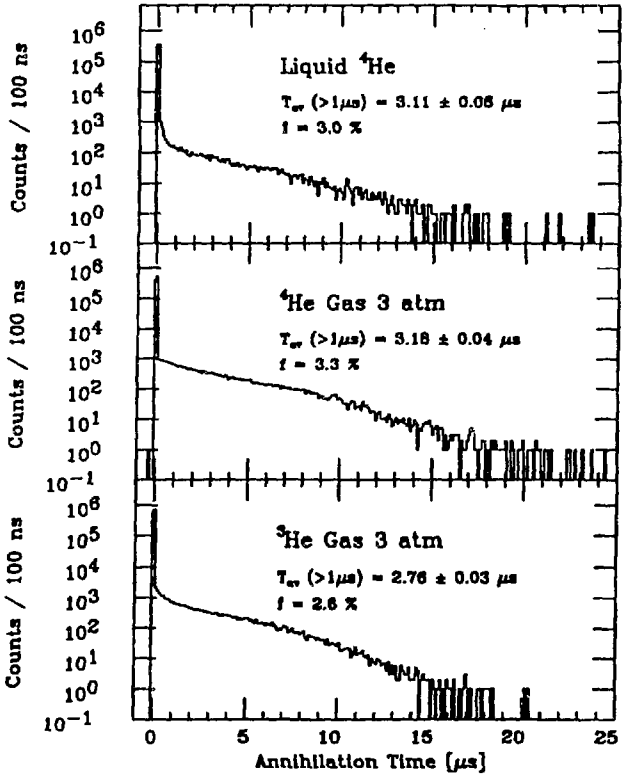

Fig. 5. Time spectra of antiproton annihilation in gas ^{4}He, gas ^{3}He, liquid ^{4}He.

The delayed fraction is unchanged, but the lifetime is shortened. This can be interpreted in terms of collision of the metastable atoms with impurity atoms/molecules. Assuming that $\bar{p}He^+$ atoms are in thermal equilibrium, we obtain the quenching cross section to be 10^{-15} cm^2 [14].

In 1992 run the PS205 group carried out more systematic and comprehensive studies of this phenomenon [15]. They measured delayed annihilation time spectra in solid He, high-pressure liquid He, low-temperature gas He, gas He with mixture of Ne, Ar, Kr, Xe, H_2, N_2, O_2, *etc.* The longest lifetime was observed in low-temperature He gas.

In 1993 we are planning to begin laser spectroscopy for the metastable states. A high-power pulsed excimer laser combined with dye laser will be used to induce resonance transition between a metastable state and a short-lived state. The proposed methodology is described by Morita *et al.* [16].

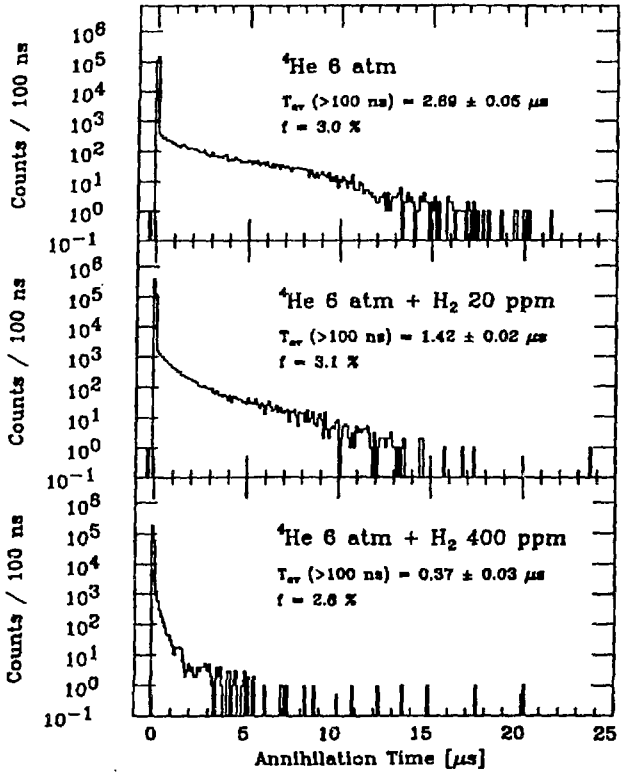

Fig. 6. Time spectra of antiproton annihilation in gas ^{4}He with mixture of H_2 gas.

4 Atomic Yrast Bands

In the following sections let us discuss the interesting features of the metastable $\bar{p}He^+$ atomcule. The most distinct aspect of this particular exotic atom that is not seen in usual atoms (even in hadronic atoms) is that it possesses large angular momenta. The metastable states can be called atomic yrast bands corresponding to the popular word for high-spin states in nuclear physics.

The usual two-body exotic atom consisting of a nucleus and an exotic particle X^- of a reduced mass M without electron contribution is described by the one-dimensional Schrödinger equation with a potential

$$U(r) = -\frac{Ze^2}{r} + \frac{l(l+1)}{2Mr^2}. \tag{9}$$

The $U(r)$ consists of an attractive long-range Coulomb potential and an repulsive short-range centrifugal potential. The potential $U(r)$ resembles a Morse potential, when the exotic particle has a large angular momentum (hence large n), and thus the system looks like a molecule, where rotational (J) and vibrational (v) quantum numbers could be uniquely assiged as $J = l$, $v = n - l - 1$, in the same way as Shimamura [17] showed in the case of the three-body system $X^- He^+$. Namely, a circular orbit ($l = n-1$) is a rotating state with a nodeless radial wavefunction, which corresponds to a vibrational quantum number $v = 0$, a next-circular state ($l = n - 2$) with a single node, corresponding to $v = 1$, and so on.

These atomic yrast states have interesting selection rules when they decay via E1 transitions; the transitions without changing the radial node are favoured, namely, $\Delta n = \Delta l = 1$. Thus, the radiative decay sequence proceeds as shown by arrows in Fig. 3, though the transitions of $\Delta n = 2$ or more have higher energies than these. This is the result of well localized radial wavefunctions in these yrast states. In the terminology of rotation-vibration we can say that a selection rule for the vibrational quantum number, $\Delta v = 0$, holds.

The Bohr orbitals do not, however, possess the usual properties of rotation and vibration; this vibrational motion is far from harmonicity and the rotational energy is not proportional to $J(J+1)$ at all (the moment of inertia is J-dependent). Here, the rotation-vibration coupling is maximal ($\hbar\omega \sim J\hbar/\mathcal{I}_{rot}$) and the moment of inertia keeps increasing with J (large centrifugal stretching). This peculiar "rotation-vibration mode" reflects the fact that the system is not like a molecule, but a Coulomb atom. In spite of this, the assignment of rotational-vibrational quantum numbers to a two-body exotic atom is a quite sufficient and useful description, although, of course, it is not a necessary one.

Now, when an electron is coupled to this large-l circular (or near-circular) orbitals, the electron motion can be treated adiabatically and the molecular approach (thus the assignment of rotation-vibration quantum numbers) does play an important role, as fully discussed by Shimamura [17]. In the adiabatic approximation the potential is now given by

$$V(R) = U(R) + \epsilon_\gamma(R) \tag{10}$$

where $\epsilon_\gamma(R)$ is the adiabatic potential arising from the electron involved. Shimamura [17] and previously Ahlrichs *et al.* [18] and recently Greenland and Thürwächter [19] solved this equation. Certainly, this molecular approach is more elegant and powerful than any other procedure starting from the atomic configurations which ought inevitably to take into account various configuration mixing effects among them. The potential shape as calculated by Shimamura is shown in Fig. 7.

Here, I would like to give some remarks on the molecular approach. Although the potential $V(R)$ looks like an interatomic Morse potential in shape, it is essentially different from the molecular case. In the present exotic helium case, the long-range attractive part comes from the Coulomb interaction and the short-range repulsion is from the centrifugal barrier, while in real molecules the long-range part comes from the molecular interatomic binding force mediated by the electron(s) and the short-range component is from the Pauli and internuclear repulsion. In the former, both the centrifugal and the Coulomb interactions together form a potential minimum where bound states are accommodated, but the electron energy $\epsilon_\gamma(R)$ is a slowly varying function which plays no

essential role in binding the two objects, and only modifies the binding energies. The effect of the electron is most elegantly and accurately taken care of by the molecular approach, but physically, the binding is essentially of "atomic origin", and as shown below, most of the results of the molecular approach as derived by Shimamura [17] such as the propensity rule ($\Delta v = 0$ dominance) do exist already in the two-body system without electron.

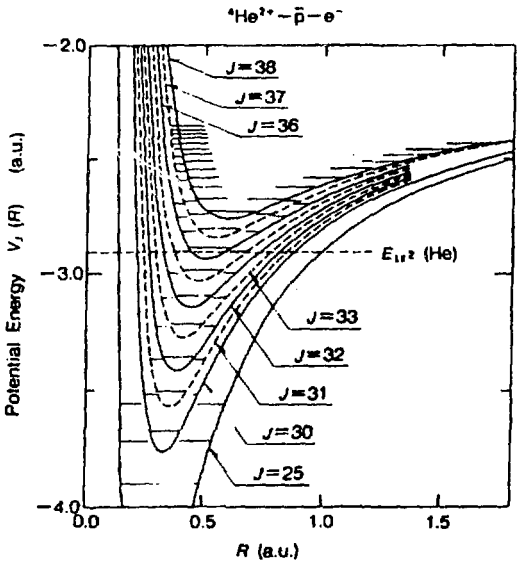

Fig. 7. Potential shape $V_J(R)$ and energy levels, as calculated by Shimamura [17].

The interesting theoretical fact that the large-l circular orbitals behave like bound states in a Morse-type potential has not manifested itself experimentally except in the case of the present metastable exotic helium atom. It is thus very interesting to consider the correspondence between the atomic approach and the molecular approach. The former is physically transparent, but mathematically troublesome and we need "perturbational" thinking. The latter is mathematically more valid, though the structure is essentially of atomic origin. Yamazaki and Ohtsuki [13] have attempted some possible discussions in a qualitative and intuitive way.

5 Atomic Core Polarization

Yamazaki and Ohtsuki [13] pointed out that there exists an effect similar to nuclear core polarization, which is a generic concept in nuclear physics, symbolizing various

phenomena in which low-energy transitions (or static moments) of multipolarity ($M\lambda$ or $E\lambda$) are enhanced or suppressed due to the coherent coupling with core excitation of the same multipolarity even if the core excitation energy is high. The most famous effect is seen in nuclear magnetic moments, as first clarified by Arima and Horie [20]. Leon and Seki [21] discussed such effects in the case of exotic atoms. Here, the core in its physical essence is not a "spatially inner" region but an "energetically deeper" region (in a nuclear system all the nucleons are confined within the same nuclear boundary, where the core implies deeper bound states, not spatially inner).

In this sense, the simplest "atomic core polarization" is seen in the present antiprotonic helium atom, where the E1 transition energies (≈ 2 eV) are by an order of magnitude smaller compared with the electronic excitation energy (≈ 18 eV). Here, the $1s$ electron constitutes the simplest core with respect to the $\bar{p}$. The important and essential point is that the residual interaction causes a special type of mixture of configurations that gives a coherent contribution to the transition rates to the first order of the mixing amplitude. This effect was not taken into account in the calculation of Russell [9], but is naturally accommodated in the molecular treatment [17–19].

The dominant configuration of $\bar{p}He^+$ of quantum numbers (N, L) is, of course, the antiprotonic $|n, l\rangle$ with the electronic $1s$; $n = N$ and $l = L$. The most important mixed configurations are the antiprotonic $|n, l\rangle = |N-1, L-1\rangle$ and $|N+1, L+1\rangle$ with the electronic np, which contribute to the transition amplitude $L \to L \pm 1$ to the first order. Yamazaki and Ohtsuki [13] calculated the mixing amplitudes defined as

$$\Psi(L+1, L) \cong \phi^{(e)}_{1s}|L+1, L\rangle_{\bar{p}} + c_L \phi^{(e)}_{2p}|L, L-1\rangle_{\bar{p}} + d_L \phi^{(e)}_{2p}|L+2, L+1\rangle_{\bar{p}} + \ldots \quad (11)$$

Specifically, the mixing coefficients are expressed by

$$c_L = -\sqrt{\frac{L}{3(2L+1)}}\left\langle \frac{r_<}{r_>^2} \right\rangle \frac{1}{\Delta E_{2p-1s}},$$

$$d_{L-1} = \sqrt{\frac{L}{3(2L-1)}}\left\langle \frac{r_<}{r_>^2} \right\rangle \frac{1}{\Delta E_{2p-1s}}. \quad (12)$$

The typical numerical values are $c_{37} = -0.127$ and $d_{36} = 0.128$. The magnitudes of these mixings are of the order of 1%. Nevertheless, the mixing causes a dramatical change in the transition rate.

The transition matrix element is in general

$$< f\|\mathbf{r}^{(1)}\|i > = < (l_e^f l_{\bar{p}}^f)L' \|\mathbf{r}_e^{(1)} + \mathbf{r}_{\bar{p}}^{(1)}\| (l_e^i l_{\bar{p}}^i)L >$$

$$= (-)^{l_e^f + l_{\bar{p}}^i + L + 1} \begin{Bmatrix} l_e^f & 1 & l_e^i \\ L & l_{\bar{p}}^i & L' \end{Bmatrix} \sqrt{(2L+1)(2L'+1)} (l_e^f \|\mathbf{r}_e^{(1)}\| l_e^i) < l_{\bar{p}}^f \mid l_{\bar{p}}^i > \quad (13)$$

$$+ (-)^{l_e^f + l_{\bar{p}}^i + L' + 1} \begin{Bmatrix} l_{\bar{p}}^f & 1 & l_{\bar{p}}^i \\ L & l_e^f & L' \end{Bmatrix} \sqrt{(2L+1)(2L'+1)} (l_{\bar{p}}^f \|\mathbf{r}_{\bar{p}}^{(1)}\| l_{\bar{p}}^i) < l_e^f \mid l_e^i >,$$

where

$$(l'\|\mathbf{r}^{(1)}\|l) = (-)^{l'} \sqrt{(2l'+1)(2l+1)} \begin{pmatrix} l' & 1 & l \\ 0 & 0 & 0 \end{pmatrix} < f'(r)|r|f(r) > \delta(l' \pm 1, l). \quad (14)$$

The unperturbed amplitude for a typical transition $(n, l) \to (n-1, l-1)$ is

$$< (s\ L-1)L-1||r_p^{(1)}||(sL)L >= -\sqrt{L} < f_{L-1}(r)|r|f_L(r) >_p \qquad (15)$$

and the first-order contribution is

$$\begin{aligned} & c_L < (s\ L-1)L-1||r_e^{(1)}||(p\ L-1)L > + d_{L-1} < (pL)L-1||r_e^{(1)}||(sL)L > \\ & = c_L\sqrt{\frac{2L+1}{3}} < s||r_e^{(1)}||p > + d_{L-1}\sqrt{\frac{2L-1}{3}} < p||r_e^{(1)}||s >, \qquad (16) \\ & = \left[-c_L\sqrt{\frac{2L+1}{3}} + d_{L-1}\sqrt{\frac{2L-1}{3}}\right] < f_{2p}(r)|r|f_{1s}(r) >_e \end{aligned}$$

which has a destructive contribution to the unperturbed amplitude.

The typical numerical value for the unperturbed amplitude is

$$< 37, 36\,||E1||\,38, 37 >_p = -3.07, \qquad (17)$$

while the 1st-order amplitude is

$$\left(-c_{37}\sqrt{\frac{2L+1}{3}} + d_{36}\sqrt{\frac{2L-1}{3}}\right) < f_{1s}(r)|r|f_{2p}(r) >_e = +1.20 \qquad (18)$$

The radial matrix element was evaluated by using the calculated basis functions. The second term gives rise to substantial reduction of the total transition amplitude, yielding a suppression factor, $1-\alpha \approx (1.87/3.07)^2 \approx 0.37$.

6 Distribution of Angular Momentum

How much is the angular momentum to be brought in exotic-atom formation? Let us make a naive and intuitive estimate. The angular momentum is given essentially by a classical estimate, namely, the momentum times the impact parameter, because the wavelength of the incoming X^- is much smaller than the collision size. The maximum angular momentum L at an incident c.m. energy E is

$$L(E) = a\sqrt{2ME}, \qquad (19)$$

with a being the maximum impact parameter. Since the bound X^- is formed most likely at a radius, which is around the electron radius, we can put $a = a_e$.

In the energy loss process of X^- the final energy of X^- at the exotic atom formation is expected to be distributed uniformly as

$$\begin{aligned} w(E) &= 1 \text{ for } E < I_0 \\ &= 0 \text{ for } E > I_0. \end{aligned} \qquad (20)$$

because the X^- of energy $E > I_0$ still undergoes ionization loss, whereas the X^- of energy $E < I_0$ forms a bound exotic atom. For a crude estimate of the initial population of l, $P(l)$, let us assume a uniform distribution of $w(E)$ below $E = I_0$.

In the simplest case of hydrogen, the maximum angular momentum for the highest energy $E \sim I_0$ becomes

$$l_{max} \cong (M/m_e)^{1/2} = n_0 \tag{21}$$

because $I_0 = me^4/2\hbar^2$ and $a_e = \hbar^2/me^2$. This is an interesting relation. Namely, it is just at $E = I_0$ that the circular orbital $l = n_0 - 1$ can be marginally populated.

For the sake of simplicity we assume that the atomic-capture cross section is given by

$$\sigma(l, E) = (2l + 1)\pi \left(\frac{\lambda}{2\pi}\right)^2 = (2l + 1)\frac{\pi}{2ME} \tag{22}$$

for

$$l < L(E) = a(2ME)^{1/2}, \tag{23}$$

where λ is the wavelength of X^-, namely,

$$\lambda = 2\pi(2ME)^{-1/2}. \tag{24}$$

This expression gives the total capture cross section to be a constant $\approx$ geometrical cross section

$$\sum_{l=0}^{l_{max}} \sigma(l, E) \approx \pi a^2. \tag{25}$$

Cohen and Padial [22] and Dolinov *et al.* [23] actually show that the formation cross section of hydrogenic and helium exotic atoms is nearly constant in the energy range $E < I_0$.

Then, the distribution $P(l)$ for a uniformly distributed energy spectrum $w(E)$ in the range $0 < E < I_0$ is

$$P(l) = \int_{E_l}^{I_0} \sigma(l, E)\frac{w(E)}{I_0} dE \tag{26}$$

with

$$E_l = \left(\frac{l}{a}\right)^2 \frac{1}{2M}$$
$$I_0 = \left(\frac{l_{max}}{a}\right)^2 \frac{1}{2M} \tag{27}$$

which leads to a simple formula

$$P(l) \propto (2l + 1)\ln(l_{max}/l). \tag{28}$$

This gives a bell shape distribution with a smooth cut off toward l_{max}. Baker [24] calculated the initial distribution $P(n, l)$ in hydrogenic exotic-atom formation and obtained a similar bell-shape form, though no clear description on the energy distribution at capture was given.

Since the energy distributes from 0 to only I_0, there is a certain limit of l; the statistical distribution of l for unlimited l is inconceivable. No precise experimental information on the initial population of l is available from any earlier experiments on exotic atoms because they are not directly related to the initial distribution of l.

Sometimes, a non-statistical distribution with a cut-off parameter, $P(l) = (2l+1)\exp(-\alpha l)$, is introduced without real justification. The above bell-shape distribution formula results from definite and reasonable physical assumptions, but the value of l_{max} is being introduced as a somewhat adjustable parameter to allow the actual l distribution to differ from the crude one given in eq.(11) as the effect of the Coulomb interaction. Theoretically better-founded formula may certainly be possible and would indeed be welcome.

The l distribution has a scaling factor $\sqrt{M}$ as n_0 and l_{max} do, and thus, the shape of $P(l)$ is a universal function of l/l_{max}. The critical angular momentum L_0 which divides the metastable and the "prompt" states (namely, a state with $l > L_0$ is metastable) can be crudely estimated as follows. i) The binding energy of the formed atomic levels of pHe^+ at $n = n_0$ (with respect to He^{++}) is roughly given by

$$E_n \approx 39.5 \frac{M}{m} \frac{1}{n^2} + 39.5 \text{ eV} \tag{29}$$

where the number 39.5 is half the total binding energy ($I_0 + 4Ry = 79$ eV) of helium atom which is assumed to be shared by X^- and e^-. The critical angular momentum is given by setting the binding energy of circular orbitals of ionized pHe^{++},

$$4 \frac{M}{m} \frac{1}{(l+1)^2} Ry, \tag{30}$$

to 79 eV, which yields

$$\frac{L_0}{n_0} \approx 0.83 \tag{31}$$

The actual critical angular momentum may be somewhat larger than this crude estimate, but what is important here is that L_0 is scaled by n_0, and thus, by $M^{1/2}$. This means that the delayed fraction is independent of the mass of X^-. This is consistent with the observation that the delayed fractions for π^-, K^- and $\bar{p}$ are all around 3 % [3–5].

7 Isotope Effect

Yamazaki and Ohtsuki [13] considered the isotope effect on the overall lifetime of He+$\bar{p}$ atom on the following grounds. Let us define the ratio of the reduced masses of $\bar{p}$ as $R = M(\bar{p}^4\mathrm{He})/M(\bar{p}^3\mathrm{He}) = 16/15$. In the atomic picture the energy spacing is approximately given by differentiating eq.(29) as

$$\Delta E \approx \frac{79}{n_0} \tag{32}$$

for the most probable $n = n_0 = (M/m)^{1/2}$. The simplest estimate using eq. (29) gives

$$\frac{\Delta E_{n_0}(^3\mathrm{He})}{\Delta E_{n_0}(^4\mathrm{He})} = R^{1/2} = 1.03 \tag{33}$$

The calculation by the molecular approach gives this ratio to be 1.025, showing that the crude estimate is not bad. The E1 matrix element depends on the reduced mass, but

as stressed in Yamazaki and Ohtsuki [13], the transition matrix element for $n = n_0$ is independent of the reduced mass. The reason is clear: the spatial distribution of $\vec{p}$ is the same at the most probable n, whatever the reduced mass is. It was shown that the unperturbed transition rates at the most likely n are the same for ^{3}He and ^{4}He. In the first-order correction the transition amplitudes remain equal to each other because the reduction factor α is independent of M. So, we consider only the M dependence of $(\Delta E)^{-3}$, giving

$$\tau_{n_0}(^4\mathrm{He})/\tau_{n_0}(^3\mathrm{He}) = R^{3/2} = 1.09. \tag{34}$$

The molecular approach gives a value, 1.09, equal to the above simple estimate.

The overall lifetime should be the typical level lifetime multiplied by an average cascade number of metastable states. Since the metastable states are expected to distribute over a given energy interval, the number of metastable cascades is proportional to the level density, namely, to $(\Delta E)^{-1}$. Multiplying this factor Yamazaki and Ohtsuki [13] obtained

$$\tau \propto (\Delta E)^{-4} \propto M^2. \tag{35}$$

This crude estimate gives $\tau(^4\mathrm{He})/\tau(^3\mathrm{He}) = R^2 = 1.13$ which turns out to agree with the recently observed value [14].

The present crude estimate may not be good, because effects other than the radiative transitions are neglected. Better theories would take into accounts Auger transitions, Stark effects, *etc.* This is an open question.

8 Deeply Bound Pionic Atoms Predicted

In 1987 Yamazaki *et al.* [25] pointed out an interesting situation for a strongly-absorptive negative hadron; it feels both the attractive long-range Coulomb potential and a short-range strong interaction. The bound states formed are not entirely "nuclear", but lie somewhere between nuclear and atomic regions. They are called "Coulomb assisted hybrid bound states". Since the negative hadron resides beyond the nuclear surface with density distribution $\rho_{nl}(r)$, the absorption width of a state nl,

$$\Gamma_{nl} = -2\int \rho_{nl}(r)W(r)d\tau \sim -2W_0\int \rho_{nl}(r), \tag{36}$$

is reduced compared with $\Gamma_0 = -2W_0$, which would be the width when the hadron were entirely confined inside the nucleus. Yamazaki *et al.* [25] suggested the existence of reasonably narrow bound states of Σ^- for some assumed potential shape. When it is repulsive, the hadron is pushed outward, and the level width is expected to be very much reduced. Such a situation may take place in the case of π^-, as Toki and Yamazaki [1] showed.

The potential parameters in the pion-nucleus interaction [26, 27] have been empirically determined by using pionic atom data (shallow atomic states). The most important fact is that the central potential is repulsive; this was indicated by small positive energy shifts of pionic atoms, observed even in pionic hydrogen atom. The absorption potential W_0 is known to have a magnitude of 10 MeV, which would mean that the expected level width is enormously large; $\Gamma_0 \sim 20$ MeV! This would be true only when the π^- were confined within the nuclear boundary.

Toki and Yamazaki [1,2] solved the Klein-Gordon equation for a negative pion bound by heavy nucleus, showing that the deeply bound states have narrow absorption widths compared with the level spacings. The calculated level scheme for π^- in ^{208}Pb is shown in Fig. 8. The reason why the level widths are so small is illustrated in Fig. 9, where the pion optical potential and the state densities $\rho_{nl}(r)$ of the $1s$, $2p$ and $2s$ states are shown. Obviously, the potential pocket around the nuclear surface accommodates those bound states. They are all *halo* states. This mechanism had been suggested by Friedman and Soff [28] who considered π^- bound states in very heavy nuclei, but it had been completely discarded in physics community. One of the reasons is the prevailing misbelief on the absorption width. Another reason is probably that they did not conceive any experimental means to detect those bound states.

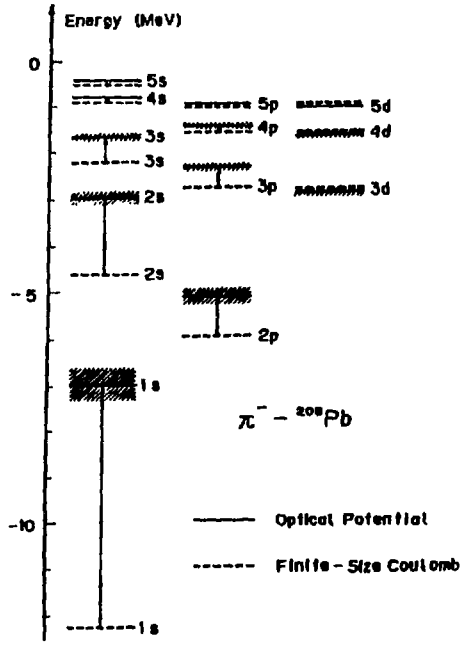

Fig. 8. Energy diagram of deeply bound pionic atom in ^{208}Pb, taken from Toki and Yamazaki [1].

9 Pion Transfer Reactions

Toki *et al.* [1,2] proposed some ways to populate those deeply bound pionic atoms, called *pion-transfer reactions*. The most straightforward idea was to make use of the

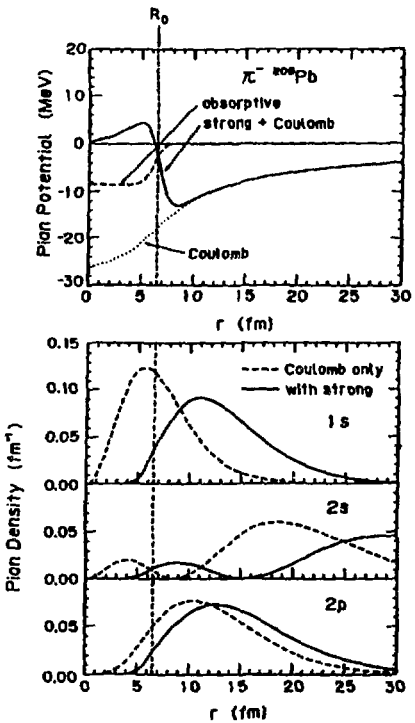

Fig. 9. The π^--nucleus optical potential for ^{208}Pb and the pion densities of the lowest three states. Taken from Toki *et al.* [2].

Yukawa vertex itself; namely, $n \rightarrow p + \pi^-$. This process does not take place in free space, because this does not satisfy the energy-momentum conservation. However, when a free neutron hits a heavy nucleus, the produced π^- can be bound by the nucleus, leaving a free proton as a spectator. Thus, in principle, this (n,p) type charge-exchange reaction produces deeply bound pionic states.

The produced states are resonance nuclear states of quantum numbers J^π satisfying $\Delta S = \Delta I = 1$, which correspond to pionic-atom quantum numbers l; $\pi = (-)^{l+1}$. The deeply bound pionic states are regarded as a new family of Gamow-Teller resonances. The (n,p) type reaction for the production of deeply bound pionic states has a large momentum transfer, q = 200 MeV/c. This makes the production cross sections very much reduced by the nuclear distortion effect [29, 30]. Search experiments have been carried out for ^{208}Pb(n,p) [29] and ^{208}Pb(d,^{2}He) [31]. Only a smoothly varying continuous spectrum was observed.

Toki *et al.* [32] have studied theoretically proton-pick-up reactions such as (n,d) and

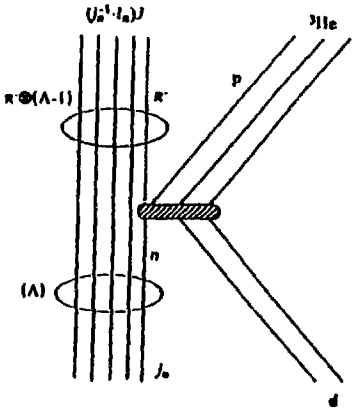

Fig. 10. Diagram for the pion-transfer (d, ^{3}He) reaction.

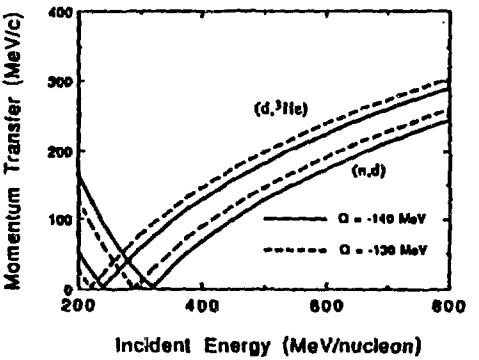

Fig. 11. Momentum transfers of (n,d) and (d, ^{3}He) reactions as functions of the incident energy.

(d,^{3}He). The diagram and the momentum transfer are presented in Fig. 10 and Fig. 11, respectively. These reactions are found to be suitable for the population of the $1s$ and $2p$ states with a neutron hole of j_n with configurations of $[(1s)_\pi \cdot j_n^{-1}]J$ and $[(2p)_\pi \cdot j_n^{-1}]J$ when the momentum transfer q matches the required angular momentum transfer, namely, $J \sim qR_\sigma$. When the matching condition is fulfilled, the distortion effect is not too large. In the (n,d) and (d, ^{3}He) reactions the momentum transfer can be tuned by selecting the incident energy. The cross sections were calculated [32] for various pionic states on the low-lying neutron hole states in ^{208}Pb, as shown in Fig. 12. The optimum energy for (d,^{3}He) leading to the $(1s)_\pi(i_{13/2})_n^{-1}$ states is 600 MeV/u. On the

other hand, at 300 MeV/*u*, where the momentum transfer is small, special pionic states of "substitutional" configurations, such as $(2p)_\pi(3p)_n^{-1}$, are preferentially populated.

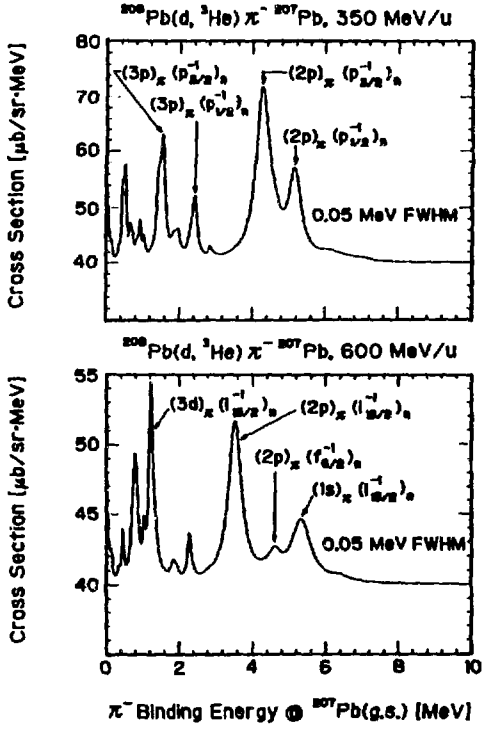

Fig. 12. Calculated ^{208}Pb(d,^{3}He) cross sections for deeply bound π^- states.

Very recently, an experiment to measure the ^{208}Pb(n,d) spectrum at excitation energies in the pion-mass region at T_n = 400 MeV has been carried out at TRIUMF [33], which showed up a large continuum characterized by the quasi-free production of π^- on a smooth background of 300 μb/sr·MeV, as shown in Fig. 13. In addition, a significant bump below the π^- emission threshold is observed. The integrated cross section over the bound π^- region is about 800 μb/sr, which is comparable with the predicted cross section. The expected spectrum in the bound π^- region is also shown in Fig. 13. Thus, this experiment gives the first experimental indication of the formation of deeply bound π^- states, but the statistics and resolution obtainable with the secondary neutron beam were not sufficient to resolve discrete peaks of the deeply-bound π^- states. To obtain further information with sufficient statistics the use of an alternative reaction (d, ^{3}He) is most desirable. The expected spectra including the quasi-free continuum have been

calculated by Hirenzaki and Toki [34].

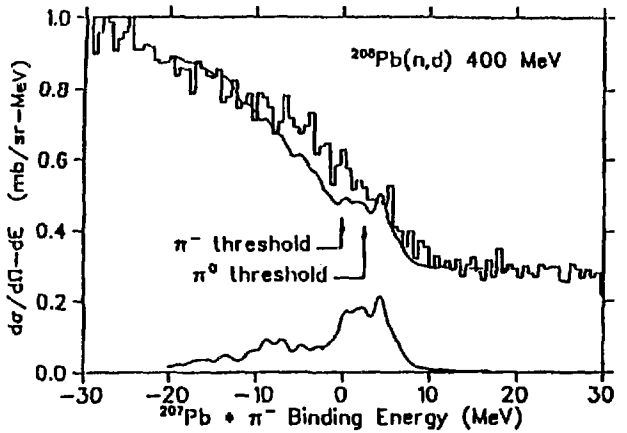

Fig. 13. Inclusive deuteron spectrum from ^{208}Pb(n,d) at 0° and 400 MeV, measured in the TRIUMF Experiment E628 by Trudel *et al.* [33]. The smooth curve is a calculation by Hirenzaki and Toki [34] for ^{208}Pb(n,d) ^{207}Pb$\otimes\pi^-$ for the pionic bound states and the free pion continuum convoluted with 1.5 MeV FWHM resolution for comparison with the data. The lower curve shows just the bound state calculation.

The Q value of the (d, ^{3}He) reaction is

$$\begin{aligned} -Q &= \omega + S_n(j_n) - [M_n + M_d - M(^3\mathrm{He})] \\ &= m_\pi - B.E.(\pi^-) + S_n(j_n) - 6.787\ \mathrm{MeV}, \end{aligned} \tag{37}$$

where ω is the excitation energy of the pionic state with respect to the neutron-hole j_n and $S_n(j_n)$ is the neutron separation energy. The four neutron orbitals, $p_{1/2}$(S_n = 7.367 MeV), $f_{5/2}$(S_n = 7.937 MeV), $p_{3/2}$(S_n = 8.246 MeV) and $i_{13/2}$(S_n = 9.000 MeV) are taken into account. Hereafter, the π^- binding energy will be defined with respect to the ground state of ^{207}Pb, and thus it corresponds to the (d, ^{3}He) reaction Q value as :

$$-Q = 140.147\ \mathrm{MeV} - B.E.(\pi^-) \tag{38}$$

The expected line profile and their angular dependence of the ^{208}Pb(d,^{3}He) reaction at T_d = 600 MeV with an instrumental resolution of 50 keV FWHM are shown in Fig. 14. It has a steep angular dependence, peaked at 0 degree. Above the π^- emission threshold there appears a quasi-free continuum, while discrete states are expected below the threshold. The constant background of ^{208}Pb (n,d) which does not contribute to the pion production has recently been measured at TRIUMF to be 300 μb/sr/MeV [30]. The constant background for (d,^{3}He) is assumed to be 40 μb/sr/MeV without angular

dependence. There is no experimental information yet on this background in the case of (d, ^{3}He).

The (d, ^{3}He) reaction has a very good intrinsic calibration coming from the two-body final state p(d, ^{3}He)π^0 when a target including hydrogen is used; the (d, ^{3}He) spectrum on a $(CH)_n$ target exhibits a distinct peak in the same momentum region as in the ^{208}Pb(d, ^{3}He) reaction. The position of this peak moves with the angle of ^{3}He.

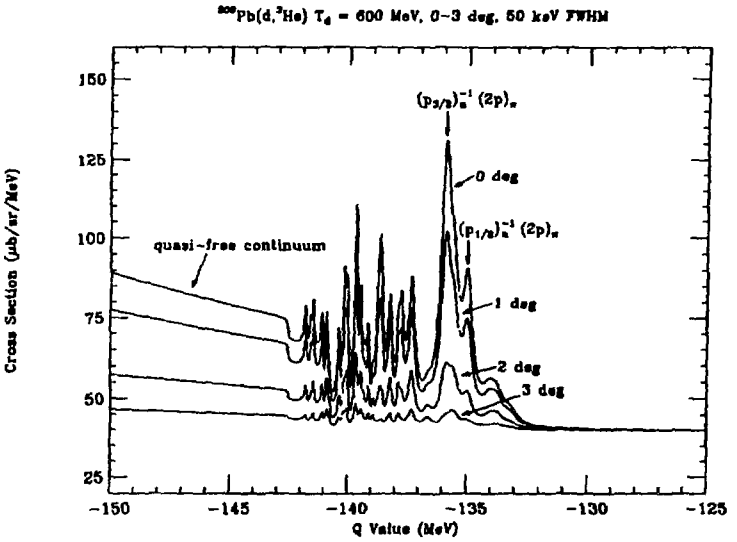

Fig. 14. Calculated spectrum and its angular dependence for ^{208}Pb(d,^{3}He) at T_d = 600 MeV with FWHM resolution of 50 keV. From the DWIA calculation of Hirenzaki and Toki [34].

Recently, a test experiment of the ^{208}Pb(d, ^{3}He) reaction was carried out at Saturne [35], where the SPES1 spectrometer system was used to detect ^{3}He particles. Although the ^{3}He particles were well identified and discriminated from other particles such as p, d and ^{4}He, the detection of (d, ^{3}He) spectrum at small angles (<3.5 deg) was prevented by a huge (d, ^{3}He) background caused by beam particles hitting the spectrometer wall. This background at small angles was difficult to suppress because the SPES1 spectrometer has a single-bend structure, while the formation cross section of deeply bound pionic states is forward peaked. It is indispensable to use a spectrometer with two (or more) bending magnets. Thus, we are proposing to measure the (d,^{3}He) reaction spectra on ^{208}Pb using the Fragment Separator [36] in combination with a deuteron beam from the SIS18 heavy-ion synchrotron of GSI.

10 Proposed (d, ^{3}He) Experiment

We propose to measure the (d, ^{3}He) reaction spectra at $T_d = 0.6$ and 1.2 GeV. The relevant kinematical quantities are shown in Table 1. We will use the Fragment Separator (FRS) system [36] with which we will measure the momentum of ^{3}He in the range of about 2 GeV/c. Since FRS is composed of 4 bending magnets, most of the background events caused by the incident deuteron beam inside the first bending magnet will be eliminated already at the intermediate focal plane, where particle tracking MWPC's and scintillation counters are placed to provide informations on p/Z, Δt and $\Delta E/\Delta x$. The particles with p/Z in a momentum bite Δp pass through these counters and are refocussed again in the final focal plane after the 3rd and 4th bending magnets. The p/Z as well as the trajectory of each particle are precisely determined by using the information from the MWPC's at the middle focal plane. At the final focal plane additional scintillation counters are placed. The combined information of the time of flight Δt and $\Delta E/\Delta x$ and p/Z is sufficient to identify individual particles.

Since the field value p/Z for ^{3}He is very close to $p_d/2$, the momentum of protons from deuteron break-up, we have to reject protons in the trigger stage to keep the trigger rate to be reasonably small. This is possible because the energy losses of the p and the ^{3}He are quite different (by a factor of 6).

A special mode for the operation of FRS [37] (large acceptance $\sim$ 3 msr and large mid-plane dispersion $\sim$ 4.2cm/%) is preferable. The overall momentum resolution of FRS including the beam momentum spread may be achieved to be 2×10^{-4}, but here, it is safely assumed to be

$$\frac{\delta p}{p} = 5 \times 10^{-4}. \tag{39}$$

This corresponds to the energy resolution in the final state after (d,^{3}He) as follows,

$$\begin{aligned} \delta\omega &= (p_{\mathrm{He}})^2/E_{\mathrm{He}} \times (\Delta p/p)_{\mathrm{He}} \\ &= 0.43 \text{ MeV for } T_d = 0.6 \text{ GeV} \\ &= 0.90 \text{ MeV for } T_d = 1.2 \text{ GeV} \end{aligned} \tag{40}$$

The resolution is deteriorated by the energy loss of the ^{3}He particle in the target. The FWHM width due to this effect is estimated to be

$$\Delta E = 6.4 \text{ keV/mg/cm}^2 \tag{41}$$

in the case of $T_d = 600$ MeV. For instance, $\Delta E = 0.32$ MeV for a 50 mg/cm^2 target. So, using this thickness, we can obtain an overall energy resolution of 0.5 MeV FWHM for $T_d = 600$ MeV. For a better resolution we have to use a thinner target at the expense of a lower event rate.

We simulated expected spectra for a typical instrumental resolution of 0.5 MeV FWHM, as shown in Fig. 15. The yield estimate assumes:

$$\begin{aligned} I_d &= 5 \times 10^{10} \text{ /sec} \\ N_{\mathrm{target}} &= 1.5 \times 10^{20} \text{ atoms/cm}^2 \text{ (50 mg/cm}^2\ ^{208}\text{Pb)} \\ \Omega &= 3 \times 10^{-3} \text{ sr } (\Delta\theta_x \sim \pm 40 \text{ mr}, \Delta\theta_y \sim \pm 20 \text{ mr}) \end{aligned} \tag{42}$$

$$\text{momentum bite } \frac{\Delta p}{p} = 0.032$$

Since the differential cross section decreases rapidly with angle, the cross section was calculated by integrating the differential cross section over the spectrometer acceptance $A(\theta_x, \theta_y)$ as

$$\sigma = \int \frac{d\sigma}{d\Omega} A(\theta_x, \theta_y) d\Omega. \tag{43}$$

They are shown in Fig. 15 (upper). Typically, $\sigma = 0.1 - 0.2\ \mu$b/MeV.

The event rate was calculated as

$$R = I_d \times N_{target} \times \sigma. \tag{44}$$

The typical value in the above condition is

$$R = 0.75 \sim 1.5 \text{ events/MeV/sec.} \tag{45}$$

The simulation presented in Fig. 15 assumes a 24-hour beam time. When the beam intensity, the spectrometer efficiency, or the calculated cross section is less than the assumed one, we have less statistics accordingly.

The energy band corresponding to the momentum bite $\Delta p/p = 0.032$ is

$$\begin{aligned} \Delta\omega &= 26 \text{ MeV for } T_d = 600 \text{ MeV} \\ \Delta\omega &= 54 \text{ MeV for } T_d = 1200 \text{ MeV}. \end{aligned} \tag{46}$$

This is very suitable in covering the energy region of present interest. We obtain 20–40 events/sec over the 26 MeV bite, which can be acquired by the present data taking system, when only the ^{3}He events were selected to trigger.

The background from break-up protons is most serious. Its yield was estimated by using the double differential cross sections given by Jafar *et al.* [38]. It is also forward peaked, and the same procedure as above was taken. The total cross section integrated over the momentum byte of the spectrometer is 50 mb. This background gives a huge counting rate in a middle-plane scintillation counter of as much as 4×10^5/sec. Taking into account the macroscopic duty factor of SIS ($\sim$0.5) we estimate the instantaneous intensity is nearly $\sim$1 MHz. The signal to background ratio is thus 1×10^{-5}. However, the energy deposit of these break-up protons is a factor of 6 smaller than that for ^{3}He.

So, we can discriminate these protons and the ^{3}He particles in the hard logic stage. We can use special drift chambers which were designed and developed for a high-rate measurement such as (π^+, K^+) reactions. Another way is to divide the mid-plane scintillation counter into several pieces.

The simulation shows that the presence of the main peaks, $(p_{1/2})_n^{-1}(2p)_\pi$ and $(p_{3/2})_n^{-1}(2p)_\pi$, will be firmly demonstrated, if they exist.

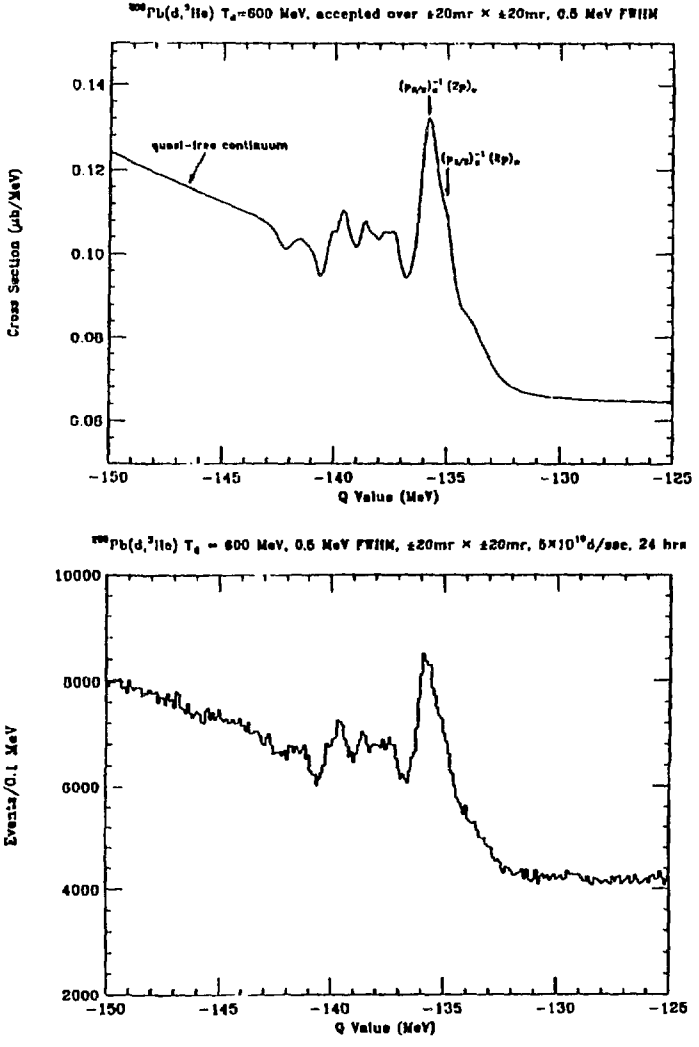

Fig. 15. Simulated ^{208}Pb(d,^{3}He) spectrum at T_d=600 MeV. A FWHM resolution of 0.5 MeV is assumed.

11 Concluding Remarks

The discovery and subsequent studies of metastable antiprotonic helium atomcules have provided a new domain of physics and chemistry. The following problems are raised, but mostly unsolved; open questions to be studied in the future.

i) Formation and structure of $\bar{p}He^+$ in very dilute medium.
ii) Structure and lifetimes of $\bar{p}He^+$ in condensed matter.
iii) Laser spectroscopy of energy levels of $\bar{p}He^+$.
iv) Photon emission spectroscopy of $\bar{p}He^+$.
v) Chemical reactions of $\bar{p}He^+$ with other atoms/molecules.
vi) Gate way to antihydrogen formation.

This interesting domain of physics and chemistry involving one baryonic antiparticle will develop in the years to come both experimentally and theoretically.

The problem of deeply-bound pionic atoms has only recently raised and it is still in a premature stage. Since it is a cluster of sharp resonance nuclear states just below the pion mass, its experimental identification will be by itself important, even surprising; it is the first nuclear state in which hadrons other than the nucleons are bound. Once this is discovered, its spectroscopy will develop, and it will be more fascinating. A high-resolution spectroscopy of deeply bound pionic atoms will provide, first of all, sets of pion bound states, which will be used to solve the question as to the potential that π^- feels from inside of the nucleus, the effective mass of π^- in nuclear medium, *etc.* It is also connected with the nuclear shape, as discussed by Toki *et al.* [39] in connection with neutron skin.

A few years ago we proposed experiments of high-resolution spectroscopy using the nuclear reactions of inverse kinematics, namely, d(^{208}Pb,π^- ^{208}Pb)^{2}He, d(^{208}Pb, π^- ^{207}Pb) ^{3}He, with a cooled beam and an internal target in the ESR of GSI [40, 41]. The proposed experiment needs more detailed consideration of beam conditions and experimental arrangements to achieve the required luminosity [42], and is thus to be realized in the future. This method will permit formation of deeply-bound pionic atoms on unstable nuclei which are circulating in a storage ring.

The author would like to thank Drs. R.S. Hayano, H. Toki, S. Hirenzaki, K. Ohtsuki, E. Widmann, J. Eades and P. Kienle for many collaborative works. The present work is supported by the Grant-in-Aid for Specially Promoted Research of Japanese Ministry of Education, Science and Culture.

References

1. H. Toki and T. Yamazaki, Phys. Lett. **B213** (1988) 129.
2. H. Toki, S. Hirenzaki, T. Yamazaki and R.S. Hayano, Nucl. Phys. **A501** (1989) 653.
3. T. Yamazaki *et al.*, Phys. Rev. Lett. **63** (1989) 1590.
4. S.N. Nakamura *et al.*, Phys. Rev. **A45** (1992) 6202.
5. M. Iwasaki *et al.*, Phys. Rev. Lett. **67** (1991) 1246.
6. R.S. Hayano *et al.*, Phys. Lett. **B231** (1989) 355.

7. R.S. Hayano, M. Iwasaki and T. Yamazaki, in *"Perspectives of Meson Science"* (ed. T. Yamazaki, K. Nakai and K. Nagamine, North-Holland, Amsterdam, (1992) Ch.13.
8. G.T. Condo, Phys. Rev. **9** (1964) 65.
9. J.E. Russell, Phys. Rev. Lett. **23** (1969) 63.
10. G. Reifenröther and E. Klemt, Nucl. Phys. **A503** (1989) 885.
11. G. Reifenröther, E. Klemt and R. Landua, Phys. Lett. **B191** (1987) 15.
12. H. Outa *et al.*, to be published.
13. T. Yamazaki and K. Ohtsuki, Phys. Rev. **A45** (1992) 7782.
14. T. Yamazaki *et al.*, Nature **361** (1993) 238.
15. E. Widmann *et al.*, Nucl. Phys. **A558** (1993) 679c.
16. N. Morita, K. Ohtsuki and T. Yamazaki, Nucl. Instr. Meth. **A330** (1993) 439,
17. I. Shimamura, Phys. Rev. **A46** (1992) 3776.
18. R. Ahlrichs, O. Dumbrajs, H. Pilkuhn and H.G. Schlaile, Z. Phys. **A306** (1982) 297.
19. P.T. Greenland and R. Thürwächter, Hyperfine Interactions, **76** (1993) 355, P.T. Greenland, private communication (1993).
20. A. Arima and H. Horie, Prog. Theor. Phys. **12** (1954) 623.
21. M. Leon and R. Seki, Nucl. Phys. **A298** (1978) 333.
22. J.S. Cohen and N.T. Padial, Phys. Rev. **A41** (1990) 3460.
23. V.K. Dolinov, G. Ya Korenman, I.V. Moskalenko and V.P. Popov, Muon Cat. Fusion 4, (1989) 169.
24. G.A. Baker, Jr., Phys. Rev. **117** (1960) 1130.
25. T. Yamazaki, R.S. Hayano, O. Morimatsu and K. Yazaki, Phys. Lett **B207** (1988) 393.
26. M. Ericson and T.E.O. Ericson, Ann. Phys. **36** (1966) 496.
27. R. Seki and K. Masutani, Phys. Rev. **C27** (1983) 2799.
28. E. Friedman and G. Soff, J. Phys. **G11** (1985) L37.
29. M. Iwasaki *et al.*, Phys. Rev. **C43** (1991) 1099.
30. J. Nieves and E. Oset, Nucl. Phys. A518 (1990) 617.
31. R.S. Hayano, in *"Pions in Nuclei"* (ed. E. Oset *et al.*, World Scientific, Singapore, 1992) p.330; R.S. Hayano *et al.*, to be published.
32. H. Toki, S. Hirenzaki and T. Yamazaki, Nucl. Phys. **A530** (1991) 679; S. Hirenzaki, H. Toki and T. Yamazaki, Phys. Rev. **C44** (1991) 2472.
33. A. Trudel *et al.*, *TRIUMF Progress Report 1991*.
34. S. Hirenzaki and H. Toki, to be published.
35. T. Yamazaki *et al.*, Saturne Proposal no.254 (1992).
36. H. Geissel *et al.*, Nucl. Instr. Meth. **B70** (1992) 286.
37. A. Schröter, PhD Thesis, Technische Universität München, July 1993 (unpublished).
38. J.D. Jafar, H.B. Van der Raay, D.G. Ryan, J.A. Stiegelmair and R.K. Tandon, Nucl. Phys. **A161** (1971) 105.
39. H. Toki, S. Hirenzaki and T. Yamazaki, Phys. Lett. **B249** (1990) 391.
40. T. Yamazaki, R.S. Hayano, H. Toki and P. Kienle, Nucl. Instr. Meth. **A292** (1990) 619.
41. T. Yamazaki, R.S. Hayano and H. Toki, Nucl. Instr. Meth. **A305** (1991) 406.
42. T. Yamazaki, *Proc. 19th INS International Symposium on Cooler Rings and their Applications* (ed. T. Katayama and A. Noda, World Scientific, Singapore, 1991) p.138.

Lecture given at the JSPS-INS International Spring School, March 1993 at Shimoda